Spectrum of Engineering Sciences
ISSN (e) 3007-3138 (p) 3007-312X Volume 3, Issue 9, 2025

TOWARDS CHIPLESS RFID TAGS FOR TAMPER EVIDENT PACKAGING APPLICATIONS

Humayun Shahid[1], Muhammad Shehryar Ahmed[2], Zain Ayaz Mughal[3], Taiba Khalil[4], Sadaf Talha[5], Bilal Ur Rehman*[6], Kifayat Ullah[7], Muhammad Amir[8]

[1,2,3,4, 5]*Department of Telecommunication Engineering, University of Engineering and Technology, Taxila, Pakistan*
[*6,7,8]*Department of Electrical Engineering, University of Engineering and Technology, Peshawar, Pakistan*

DOI: https://doi.org/10.5281/zenodo.17189277

Keywords
Chipless Tags, Smart Packaging, Radio Frequency Identification, Tamper Evident, Chipless RFID Applications

Article History
Received: 25 June 2025
Accepted: 03 September 2025
Published: 15 September 2025

Corresponding Author: *
Bilal Ur Rehman

Abstract
This paper addresses the need for low-cost, tamper-evident identification tag within regulated supply chains by advancing a chipless radio-frequency identification approach that encodes information in the scattering spectrum of printable resonant structures. The proposed tag comprises eight concentric hexagram resonators patterned in conductive ink on a polyethylene terephthalate substrate, forming a 10 × 10 mm² label that yields an unambiguous 8-bit signature via eight well-separated attenuation minima in the radar cross-section spectrum across 7–20 GHz. With the help of commercially available state-of-the-art full-wave electromagentic simulation software, this study characterizes the normal and tampered state produced by the electronic equivalent of physical tampering of the tag. Tampering suppresses specific modes and shifts the remaining resonances—reducing the code to six notches displaced toward higher frequencies—thus enabling simple decision rules based on notch count, depth, and frequency shift to detect compromise. The results demonstrate a pathway from laboratory concepts to scalable, passive, and fully-printable tamper evident packaging with built-in chipless RFID tag structures that can unify identification with integrity monitoring in pharmaceuticals, food, and high-value parts.

INTRODUCTION

Contemporary, globally sourced supply chains rely on a fragile infrastructure of trust: products can be sent through multilayered logistics without being adulterated, diverted or substituted, but the artefacts of verification used in practice, such as inked seals, serial stickers, and even many silicon-based RFID/NFC tags, are either easy to counterfeit or outrageously expensive to use on a ubiquitous basis. Chipless RFID provides an appealing way out in this regard. It retains the important properties of radio identification that include non-line-of-sight readability and automated item identification whilst eliminating silicon by storing information in the electromagnetic scattering response of a structure. No longer tied to integrated circuitry, the tags can be printed, rendered at extremely low cost, formed to curved or flexible packages, and work without an onboard power source. Furthermore, the spectrograms of their resonant architecture can be deliberately crafted to expose compromise: tears, cuts, or delamination permanently alter the spectral code, and this can be used to signal compromise, a machine-checkable signal, [1], [4]– [6], [8], [9], [12].

Frequency-coded chipless identifiers in this paradigm encode digital data via the presence, spectral location, and geometrical nature of notches in the radar cross-section (RCS) response. A reader interrogates an ultra-wideband (UWB) stimulus; the tag features engineered resonators that re-radiate a signature, where each notch corresponds to a bit or symbol. More recently, analytical modeling and detectors based on notches have elucidated the dependence of

identification fidelity on the quality factor (Q), notch depth, and frequency placement, as well as how tolerances in fabrication or environmental variations can dislocate the code in predictable patterns [2], [3]. The insights are twice valuable in the context of tamper evidentiation: the same sensitivities that frustrate robust decoding with benign variability can be used to cause harm, as long as we can distinguish between harmful and harmless perturbations using signal design and reader processing [2], [9], [15].

Process engineering and materials selection are both determinative of performance. Printable conductors (silver nanoparticle inks, aluminium, and carbon/graphene composites are increasingly popular) are deposited on flexible dielectrics (PET, paper, polyimide support roll) to support roll-to-roll manufacture, low-temperature process, and conform accurately to non-planar packaging. The electromagnetic budget is, however, ultimately determined by coupled physical parameters: ohmic loss and current crowding are controlled by sheet resistance (RsquareRsquareRsquare); effective conductivity close to the skin depth is determined by surface morphology and roughness; stored energy versus dissipated energy is determined by dielectric properties of the substrate, especially loss tangent and dispersion. Combined, these aspects determine the usable resonator quality factor and notch depth, hence the usable read range, spectral selectivity, and sensitivity of the code to perturbation [11], [17].

More recent surveys of flexible and printed RF structures have been accompanied by comparative studies across various ink chemistries, deposition processes (screen, gravure, or inkjet), and curing conditions (thermal, photonic, or hybrid), which have quantified these trade-offs with greater precision. Process-aware synthesis, which includes workflows that integrate Taguchi design-of-experiments with population-based optimizers, has been particularly successful in exploring the coupled design space. With explicit accounting of fabrication tolerances, inter-resonator coupling, and substrate anisotropy in the objective function, such techniques achieve spectral notches at selected frequencies at sub-percent error and maintain sufficient inter-notch isolation [7], [11]. More importantly, the combination of materials science and electromagnetic design provides an effective stick in the mud of tamper evidence. Movies with almost percolated thresholds or run with narrow loss margins can produce bits that are fragile, spectroscopically isolated spectral features, the appearance of which is sensitive to microstructural integrity. These engineered notches undergo predictable attenuation, drift, or coalescence in the presence of incipient damage (micro-cracks, partial tears, or adhesive delamination) and transform minute mechanical insults into machine-readable spectral events. Thus, manufacturing decisions do not just limit performance; they can be used to design tags on architects whose electromagnetic signatures are consistently informative signals of concession, [15], [18].

Simultaneously, numerous developments in intelligent packaging indicate that it is following a path from straightforward identification to genuine authenticity and integrity surveillance, enhanced with sensing. RFID platforms have been hybridised with humidity-, temperature-, strain-, and gas-sensing foils and functional inks to capture exposure histories, indicate abusive handling, and support condition-sensitive verification [5], [6], [9]. Within such architectures, the transduction layer disturbs the electromagnetic response in a controlled way, and provides a fingerprint of tamper- and environment-sensitive response, instead of a fixed identifier [12], [16].

This change is powerful in chipless applications. Tiny labels with onboard resonators (up to a dozen or more) now show not just high identification capabilities but also continuous multi-sensor density in the footprint of about 1520 mm. The engineered resonant constellation exhibits measurable diagnostic spectral shifts, such as changes in notch frequency, depth, or linewidth, which have a direct mapping to the sensed variable under environmental stimuli. The outcome is a low-cost, co-printable modality where identification and condition monitoring are co-encoded in the backscattered spectrum, enabling provenance, quality assurance, and tamper-evidentiation by the same passive tag. Tamper evidentiation is based on the same physical principles: mechanical perturbation alters currents and effective permittivity, generating unrecoverable notch loss, frequency shift, or Q-degradation subject to codification into decision rules [5], [6], [8], [9].

Although these improvements have been made, scale implementation in the regulated supply chain continues to be limited by four intractable shortcomings. Such exceptional deficiencies, both structural and methodological in nature, remain restrictive of robustness, interoperability, and compliance-readiness, thereby moderating real-world implementation. They need to be dealt with strategically in order to translate laboratory demonstrations into acceptable, verifiable practice. First, metrics and tamper taxonomies are still not well specified. Not many studies specify standardized classes of damage, such as clean cuts, partial tears, adhesive peels, and punctures, and state ROC-style performance with angle/polarization sweeps and realistic clutter. Second, under-characterized failure modes in frequency-coded tags: Reader robustness to variable incidence, polarization mismatch, and near-field coupling with package contents are under-characterized failure modes [2], [3], [9]. Third, aging and environmental quashing, as well as micro-cracking of inks, abrasion, can lead to tampering. The association of aging in printed electronics and flexible antenna research with quantitative code drift has become a topic of interest only recently [7], [11], [17]. Fourth, security and unclonability are strategic: anti-counterfeit seals are advantaged by physically unclonable spectral fingerprints, but practical enrollment/readout that can survive field conditions remains immature [14].

The current work anchored in the attached thesis fills these gaps by (i) reducing the geometry of the tamper to a compact, printable, multi-resonator geometry, that is optimized to enhance discontinuities caused by fractures; (ii) formalizing the tamper scenarios-clean shear, partial tear, peel, puncture-mapped to quantifiable spectral responses (notch count loss, center-frequency shift, and Q-reduction) and their bit-error implications; and (iii) assessing robustness of interrogation in polarization/angle sweeps. The previous prototype (10 10 mm PET, silver-ink metallization, eight resonators between 720 GHz) already achieved clear before/after codes when separated mechanically; here, we build on that base with standard damage taxonomies, environment-stress conditions, and decision levels applicable to portal or handheld readers in the logistics environment. This path is expected to transform chipless RFID from a laboratory concept to scalable tamper-evident seals on pharmaceuticals, food, and high-value parts in the field.

LITERATURE REVIEW

The state of chipless RFID, with a particular focus on frequency-coded notches as a route to ultra-low-cost identification and an enumeration of the continuing impediments, was synthesized by Herrojo et al. [1]. Based on this, Alam/Shah and others developed a notch analytical model that produces a correlation between the Q-factor and spectral placement, providing quantitative insight into code integrity under variability [2]. In parallel, Vena, Perret, and Tedjini showed high-coding-capacity frequency-spectra designs and described reader architectures and calibration schemes that trade density and robustness [3]. In volumetric and mechanically-resilient applications, Terranova et al. investigated additive-manufactured 3-D chipless tags, which, though inefficient in tamper, demonstrate manufacturability and spectral control over planar prints [4].

A 2024 review describes the direct dependence of process parameters on RCS and notch depth by controlling the conductivity of inks, the thickness of layers, and surface morphology to control the performance of antenna and resonator devices on PET and polyimide [7]. More exhaustive evaluations of printed electronics and packaging-substrate analysis introduce the context of cost and durability, e.g., silver-ink cost limitations, trade-offs, and packaging-substrate implications of curing profiles on long-term stability [11], [17]. In the design-automation perspective, design-recent letters have suggested Taguchi-initialized PSO to introduce notches at desired frequencies even when resonators couple, a method here to co-opt, at the expense of engineering fragile bits that are prone to code erasure when subjected to minor structural insults [18].

RFID sensing [5] and innovative packaging [12], [16] reviews describe a shift toward the ID to exposure logging (humidity, temperature, gas), and silicon-free chipless versions providing sensing. Compact, data-dense tags, such as the 20-bit moisture-sensing design of Jabeen et al. [8] and a 29-resonator PET laminate that incorporates moisture and temperature sensing in a 15 × 16 mm² area [6], [7], are exemplary chipless implementations. Parallelly, Mc Gee et al. examined

structural health contexts (strain and temperature) and interrogation bandwidth/data resolution requirements of sound sensing, yielding findings that can be immediately applied in tamper discrimination with clutter and angle/polarization variations [9], [10].
In the case of high-value goods, anti-cloning plays a key role. Yang, Tehranipoor, and Forte suggested unclonable, environmentally sensitive chipless tags whose spectral responses serve as physically unclonable functions (PUFs) to form unique IDs that also drift when subjected to environmental stimuli-conceptually similar to our goal of tamper-revealing fingerprints [14]. In the meantime, frequency-selective-surface (FSS)-based security paper shows how engineered reflectivity can be a strong authenticity cue at portal gates, which supports spectral selectivity as a powerful integrity-checking cue [13].
Mohonta et al. (in the recent review of the strain-sensor that does not rely on a chipless mechanism) classify mechanisms and materials, pointing out that silver inks and flexible substrates provide low loss and consistent sensitivity, material evidence that mechanical perturbations can be made diagnostic in spectral space [15]. The combination of these studies, with notch-modeling work [2] and SHM demonstrations [9], [10], posit that a standardized tamper taxonomy and ROC-style benchmarking should report bit-loss, center-frequency migration, and Q-degradation thresholds at controlled damage and environmental confounders.
Screen-print analyses highlight constraints and opportunities of chipless structures on foil and paper, such as ink cracking and adhesion that age with time and moisture, and are affected by handling phenomena explicitly monitored by our protocol [11], [17]. Recent survey papers with a materials focus also list graphene/aluminum as cost-sensitive alternatives to silver inks, reporting the conductivity penalty and process control requirements necessary to maintain Q-factors [15].
Literature confirms (i) that frequency-coded chipless tags are feasible, printable, and high-capacity; (ii) that notch physics and process parameters can be designed with fine granularity; and (iii) that mechanical/environmental perturbations can be realized as structured spectral changes, which are detectable and measurable. What remains is a tamper-resistant methodology that combines fragility-conscious tag design with reader-side robustness and metrics that distinguish between damage and drift. Hence, it is precisely the scaffolding that the present work provides, based on the thesis prototype as an empirical anchor, and extending it to a field-minded system of tamper evidence.

GEOMETRIC DESIGN AND CONFIRGURATION OF PROPOSED TAG:

We propose a frequency-coded tag based on a concentric hexagram topology. Eight resonant inclusions, meticulously patterned on the dielectric substrate, engineer the backscattered radar-cross-section spectrum to exhibit eight discrete, high-contrast spectral features (notches/peaks). Each feature functions as an unambiguous information bit, yielding a readily identifiable 8-bit signature in the RCS response.

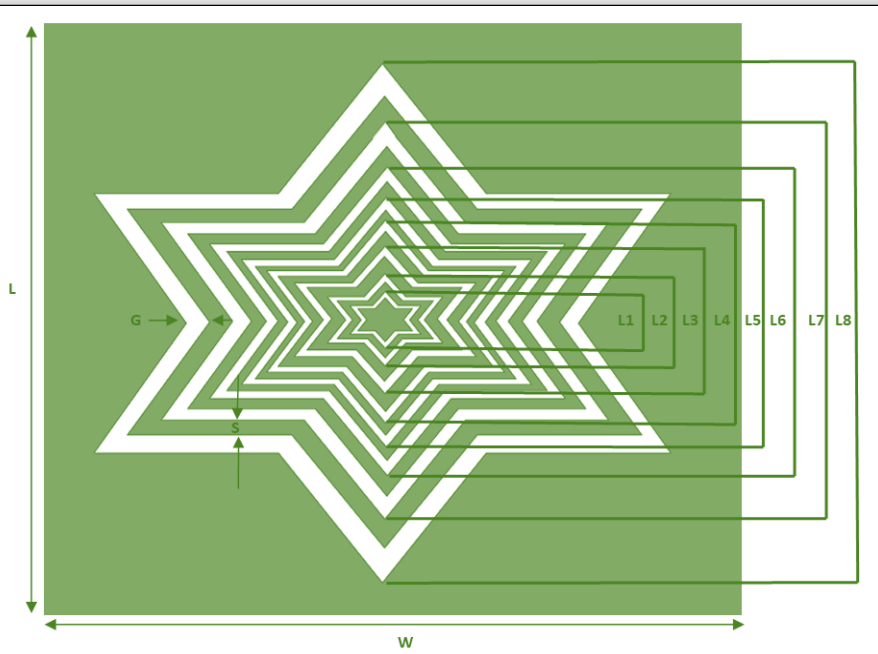

Figure 01: Front View - Proposed Concentric Hexagram Configuration of the Tamper Evident Tag

The substrate selection aligns with prevailing practices in large-scale production of tamper-evident packaging, for which polyethylene terephthalate (PET) is the de facto dielectric of choice. We employ a thin, flexible PET film characterized by a relative permittivity $\varepsilon_r \approx 2.9$ and a loss tangent $\tan\delta \approx 0.025$. The tag footprint is compact—10 × 10 mm²—and the conductive pattern is realized on the upper surface using silver-based conductive ink.

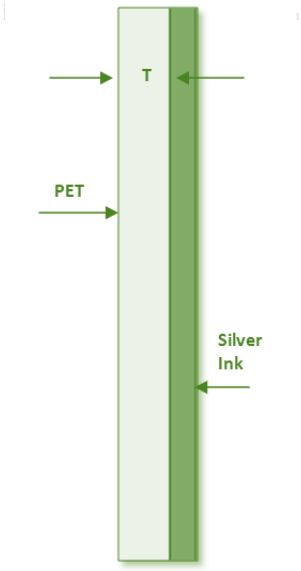

Figure 02: Side View - Proposed Concentric Hexagram Configuration of the Tamper Evident Tag

As shown in Figure 01, the tag comprises eight concentric, Hexagram resonators. These resonant apertures are defined by selectively ablating the silver conductive layer on the tag's upper surface, thereby patterning the dielectric to realize the desired topology. Each resonator contributes a distinct

spectral feature to the backscattered frequency response, collectively encoding an unambiguous 8-bit signature. Geometric parameters are held consistently across the array in its entirety: the resonator trace width and inter-element spacing are fixed at G and S, respectively; individual resonator dimensions are specified by their length LZ where Z ranges from 1 all the way to 8 representing the inner-most to the outermost resonant element. The substrate thickness, as shown in Figure 02, is denoted by T, whereas the overall width and length of the tag is denoted by W and L respectively. The complete set of design parameters is summarized in Table 01.

Table 01: Design parameters for proposed tamper evident tag

Parameter	Description	Value (mm)
L	Length of Tag	10
W	Width of Tag	10
G	Gap to Resonator	0.18
S	Spacing between Resonators	0.18
L1	Length of 1st Hexagram	4.56
L2	Length of 2nd Hexagram	5.28
L3	Length of 3rd Hexagram	6
L4	Length of 4th Hexagram	6.72
L5	Length of 5th Hexagram	7.44
L6	Length of 6th Hexagram	8.16
L7	Length of 7th Hexagram	8.88
L8	Length of 8th Hexagram	9.60

RESULTS AND DISCUSSION: NORMAL STATE

The proposed architecture was evaluated numerically in CST Studio Suite, wherein full-wave electromagnetic simulations were used to predict the tag's backscatter characteristics. The radar cross-section (RCS) was extracted from the simulated fields using a calibrated field-probe post-processing workflow, yielding a frequency-resolved backscatter spectrum for the complete structure. The resulting RCS profile is depicted in Figure 03 and provides a compact yet informative summary of the tag's scattering behavior across the operational band.

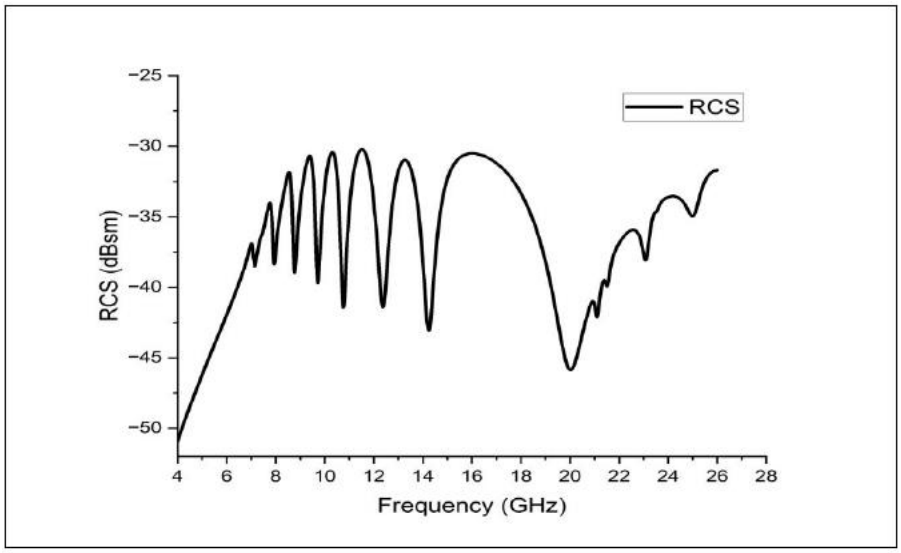

Figure 03: Spectral response of the proposed tag in normal state depicting 08 spectral dips.

The actual distribution of the proposed tag is shown in Figure 04. The current distribution of a single hexagram star resonator indicates maximum concentration in the lateral arms, and weaker currents on the top and bottom of the arms. This will verify that the side arms play the dominant role in the resonance behavior by comprising the main current paths, while the top and bottom arms play the key role in the frequency tuning and coupling behavior. Such peculiarly manifesting current distribution enhances the resonance strength and thus deeper RCS notches are obtained.

Across the 7–20 GHz span, the simulated response exhibits eight well-separated attenuation minima (resonant "notches"), each arising from an individual hexagram resonator and therefore mapping one-to-one onto the intended code elements. The notches are spectrally distinct and sufficiently spaced to preclude overlap, which facilitates unambiguous identification during readout and mitigates classification errors in practical interrogation scenarios. In aggregate, these features constitute an 8-bit frequency-domain signature embedded directly in the backscattered RCS, thereby substantiating the design's frequency-coded encoding paradigm.

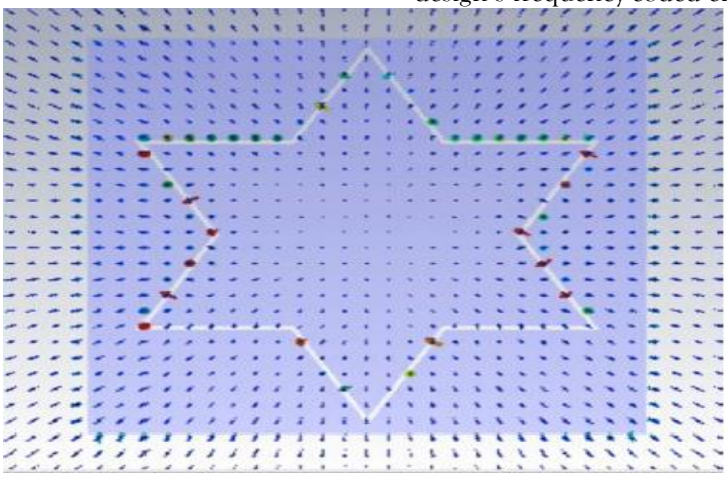

Figure 04: Surface current distribution across a single hexagram star resonant element

Equally important, the depths of all resonant notches remain appreciably high over the entire band of interest, providing robust contrast against the surrounding spectral baseline. This depth ensures reliable detection under typical signal-to-noise conditions and affords comfortable margin with respect to standard thresholding strategies used in frequency-coded tag readers. Taken together, the simulated results corroborate the intended operating principle: each resonator contributes a unique, readily discernible spectral landmark, and their ensemble realises a compact, stable, and machine-decodable 8-bit RCS signature.

RESULTS AND DISCUSSION: TAMPERED STATE

To evaluate tamper-evidence, we re-simulated the structure after mechanically partitioning the tag into two halves, thereby emulating a representative breach of package integrity of the tag as seen in Figure 05. Full-wave analyses were repeated under identical excitation and boundary conditions so that any deviations in the backscattered response could be attributed solely to the induced structural discontinuity. This intervention disrupts the continuous current paths and inter-resonator coupling that underpin the designed scattering behaviour, and thus provides a stringent test of the encoding scheme's physical robustness.

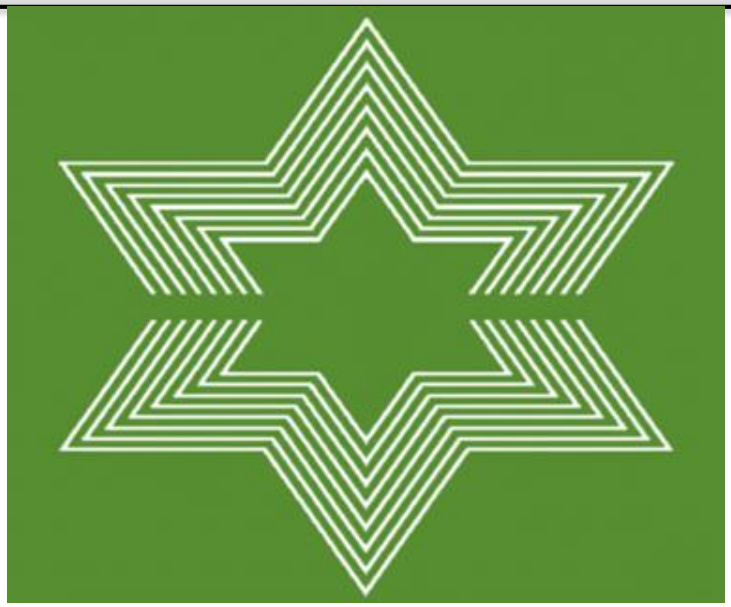

Figure 05: Proposed tamper evident tag in the tampered state

The corresponding radar cross-section spectra as shown in Figure 06 reveal a decisive transformation of the frequency-coded signature. Several resonant landmarks vanish entirely, while the surviving features reorganize both in number and in placement: the constellation of notches is reduced to six and the residual minima are displaced within the higher band, spanning approximately 14–25.5 GHz.

The selective disappearance of modes reflects the loss of specific hexagram resonators from the effective circuit, whereas the systematic shift of the remaining resonances indicates altered electromagnetic coupling and modified effective electrical lengths following the break. Together, these changes yield a signature that is not only degraded but qualitatively different from the pristine 8-bit code.

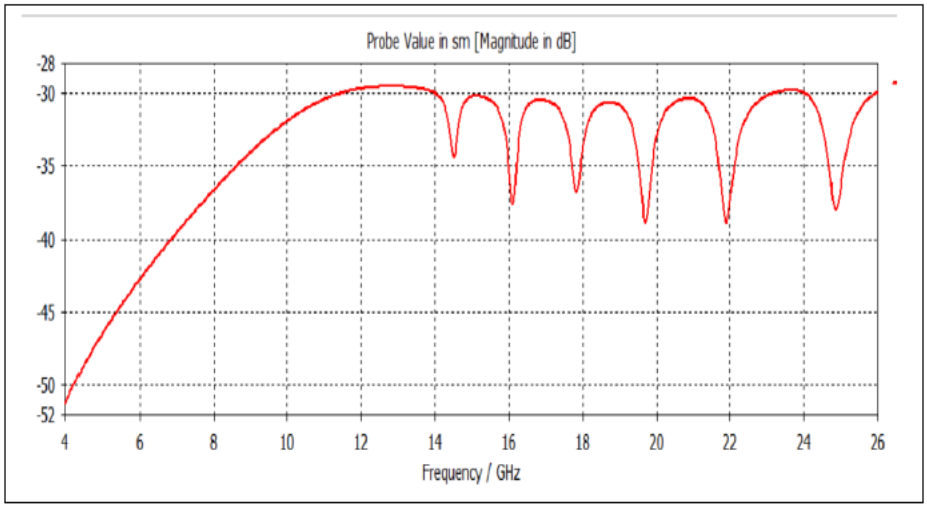

Figure 06: Spectral response of the proposed tag in tampered state depicting 06 spectral dips.

Critically, because the information content is inseparably tied to the physical ensemble of resonators, any tampering that severs or distorts these elements perturbs the spectral fingerprint in a manner that is both predictable and machine-detectable. In practical terms, straightforward decision rules—such as thresholding on notch depth, counting the number of resolvable minima, or evaluating a Hamming-like

distance in the frequency domain—can flag compromised tags with high confidence. These results substantiate the tag's intrinsic tamper-evident functionality and underscore its utility for anti-counterfeit assurance in mass-produced packaging.

CONCLUSION

This research develops and tests by simulation a tamper evident tag based on a printable frequency coded chipless tag for logistics environments. An eight resonator, concentric hexagram topology, on a flexible packaging substrate generates a stable, well spaced, 8-bit spectral signature in the normal state, as verified by full wave simulation of the radar cross-section. When the tag is mechanically cut to simulate a realistic breach, the encoded constellation will degrade in a predictable way: some notches will disappear while others will migrate to higher frequencies, giving a qualitatively different six-feature spectrum. Because the information content cannot be separated from the physical resonator ensemble, very simple decision rules, such as thresholding on notch depth, counting resolvable minima, or calculating a frequency domain distance can flag compromise with a high degree of confidence. These results support the key assertion that process-aware electromagnetic design can transform extremely small structural insults into machine-readable spectral events for low-cost, passive seals that can combine item identification with integrity surveillance. Because the information content is inseparable from the physical resonator ensemble, rather simple decision rules, as in thresholding on the depth of a notch, counting resolvable minima or calculating a frequency domain distance can identify compromise with a high degree of certainty. These results support the key assertion that process-aware electromagnetic design can enable extreme small structural insults to be transformed into machine-readable spectral events for the low-cost and passive seals that can combine item identification with integrity surveillance.

REFERENCES:

[1] C. Herrojo et al., "Chipless-RFID: A review and recent developments," Sensors, vol. 19, no. 15, p. 3385, 2019, doi: 10.3390/s19153385. (MDPI)

[2] J. Alam, M. Khaliel, A. Fawky and A. El-Awarmy, "Frequency-coded chipless RFID tags: Notch model, detection, angular orientation and coverage measurements," Sensors, vol. 20, no. 7, p. 1843, 2020, doi: 10.3390/s20071843. (MDPI)

[3] K. Mekki, O. Necibi, H. Denis, P. Medis and A. Gharsallah, "Frequency-spectra-based high coding capacity chipless RFID using an UWB-IR Approach," Sensors, vol. 21, no. 7, p. 2525, 2021, doi: 10.3390/s21072525. (MDPI)

[4] S. Terranova, F. Costa, G. Manara, and S. Genovesi, "Three-dimensional chipless RFID tags: Fabrication through additive manufacturing," Sensors, vol. 20, no. 17, p. 4740, 2020, doi: 10.3390/s20174740. (MDPI)

[5] F. Costa, S. Genovesi, M. Borgese, A. Michele, F. A. Dicandia and G. Manara, "A review of RFID sensors, the new frontier of Internet of Things," Sensors, vol. 21, no. 9, p. 3138, 2021, doi: 10.3390/s21093138. (MDPI)

[6] V. Mulloni, G. Marchi, A. Gaiardo, M. Valt, M. Donelli and L. Lorenzelli, "Applications of chipless RFID humidity sensors to smart packaging," Sensors, vol. 24, no. 9, p. 2879, 2024, doi: 10.3390/s24092879. (MDPI)

[7] M. N. Hamidon, T. D. Farnana, I. H. Hasan, A. Sali, and M. Md. Isa, "Printing of passive RFID tag antennas on flexible substrates: Materials and techniques," Journal of science: Advanced materials and devices, vol. 9, no. 4, p.100778, 2024, doi: 10.1016/j.jsamd.2024.100778. (ScienceDirect)

[8] I. Jabeen, A. Ejaz, M. U. Rehman, M. Naghshvarianjahromi, M. J. Khan, Y. Amin and H. Tenhunen, "Data-dense and miniature chipless moisture sensor RFID tag," Electronics, vol. 8, no. 10, p. 1182, 2019, doi: 10.3390/electronics8101182. (MDPI)

[9] K. Mc Gee, P. Anandarajah and David Collins, "Use of chipless RFID as a passive, printable sensor for Aerospace Strain and Temperature Monitoring," Sensors, vol. 22, no. 22, p. 8681, 2022, doi: 10.3390/s22228681. (MDPI)

[10] K. Mc Gee, P. Anandarajah, and P. T. Callaghan, "Proof-of-concept novel configurable chipless RFID strain sensor," Sensors, vol. 21, no. 18, p. 6224, 2021, doi: 10.3390/s21186224. (MDPI)

[11] M. Švanda, J. Machac and M. Polivka, "Constraints of using conductive screen-printing for Chipless RFID Tags with Enhanced RCS Response," Applied Sciences, vol. 13, no. 1, p. 148, 2022, doi: 10.3390/app13010148. (MDPI)

[12] L. Wang, Z. Wu, and C. Cao, "Technologies and fabrication of intelligent packaging for perishable products," Applied Sciences, vol. 9, no. 22, p. 4858, 2019, doi: 10.3390/app9224858. (MDPI)

[13] S.-H. Lee, M.-S. Kim, J.-K. Kim and I.-P. Hong, "Design of security paper with Selective Frequency Reflection Characteristics," Sensors, vol. 18, no. 7, p. 2263, 2018, doi: 10.3390/s18072263. (MDPI)

[14] K. Yang, U. J. Botero, H. T. Shen, D. L. Woodard, D. Forte, and M. M. Tehranipoor, "UCR: An unclonable environmentally sensitive chipless RFID tag for protecting supply chain," *ACM Transactions on Design Automation of Electronic Systems*, vol. 23, no. 6, Nov. 2018, doi: 10.1145/3264658. (tehranipoor.ece.ufl.edu)

[15] S. C. Mohonta, N. Banerjee, and A. Bhattacharya, "Chipless RFID strain sensors: A review and performance analysis," *Sensors and Actuators A: Physical*, vol. 371, p. 115647, 2024, doi: 10.1016/j.sna.2024.114046. (ScienceDirect)

[16] J. Zuo, J. Feng, M. G. Gameiro, Y. Tian, J. Liang, Y. Wang, J. Ding, and Q. He, "RFID-based sensing in smart packaging for food applications: A review," Future Foods, vol. 6, p. 100198, Oct. 2022, doi: 10.1016/j.fufo.2022.100198.(PubMed)

[17] P. Fathi, S. Shrestha, R. Yerramilli, N. Karmakar, and S. Bhattacharya, "Screen-printed chipless RFID tags on packaging substrates," *Flexible and Printed Electronics*, vol. 6, no. 2, p. 025009, Jun. 2021, doi: 10.1088/2058-8585/ac03be. (Research Management)

[18] C.-C. Le, T.-K. Dao, N.-Y. Pham, and T.-H. Nguyen, "Encoding capacity enhancement for chipless RFID tag using resonant frequency placement," IEEE Access, vol. 11, pp. 117907–117919, 2023, doi: 10.1109/ACCESS.2023.3326253.

[19] M. Nadeem, A. Habib, and M. Y. Umair, "Chipless RFID based multi-sensor tag for printed electronics," *Heliyon*, vol. 10, no. 4, Art. no. e26494, Feb. 2024, doi: 10.1016/j.heliyon.2024.e26494. (ScienceDirect)

[20] H. Anam, S. M. Abbas, I. B. Collings, and S. C. Mukhopadhyay, "A PDMS/MWCNTs RFID flexible tag with advanced resonator design for read-range enhancement in IoT monitoring systems," Scientific Reports, vol. 15, p. 9686, 2025, doi: 10.1038/s41598-025-86773-7. (Nature)